THE JOURNAL OF PHYSICAL CHEMISTRY C

Article

Cite This: J. Phys. Chem. C 2018, 122, 20727−20735

pubs.acs.org/JPCC

Molecular Simulations of Binary Gas Mixture Transport and Separation in Slit Nanopores

Tianhao Wu and Abbas Firoozabadi*

Reservoir Engineering Research Institute, 595 Lytton Avenue Suite B, Palo Alto, California 94301, United States

Supporting Information

ABSTRACT: We propose a new method to simulate the gas mixture transport and separation in slit nanopores. The method is based on the random removal of molecules from the permeate side in the dual control volume−grand canonical molecular dynamics (DCV-GCMD) method. Each step in the random removal is independent of the previous steps. The conventional method, DCV-GCMD, simulates the gas mixture in control volumes based on the chemical potential of each component, in which the gas compositions have to be known in advance and kept constant. However, the transport process affects the composition of the produced gas mixture due to selective adsorption in the nanopores. This process has been modeled iteratively in the literature. We propose an alternative method to calculate the composition in the permeate side directly; in our approach, the computational efficiency is improved by an order of magnitude compared to the iterative method. Transport of gas mixtures of CH_4/He and CO_2/CH_4 is investigated in graphene, graphite, and tetrahedral−octahedral−tetrahedral (TOT) structure slit pores. Pore width is the dominant factor in the species separation. The solid substrates and surface roughness have a pronounced effect on gas separation. The average pressure may have a pronounced effect when the pore width is less than 1.00 nm.

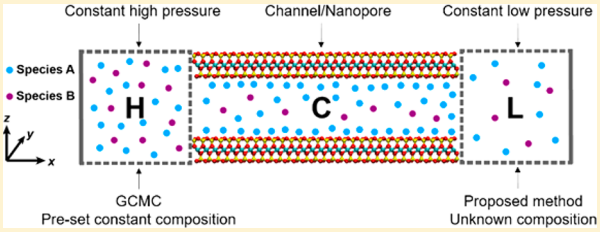

INTRODUCTION

Gas mixture transport through nanopores is a classic topic and of great interest. The porous materials, with pore scales ranging from micropores to mesopores, are widely utilized in adsorption and gas separation, including natural gas sweetening, flue gas purification, gas storage, carbon dioxide capture, and shale gas development.[1−5] In gas separation, various parameters affect the transport and separation of species, including the molecular size, the pore geometry and connectivity, and the interactions between the molecules and the pore surface.[1,2,6] In shale gas formations, due to the nanometer size of pores, there may be a separation of species at high pressure. The investigation of the mechanisms will shed light on the gas transport and separation and the engineering of the material design accordingly.

The grand canonical Monte Carlo (GCMC) simulation has been widely applied to investigate the selectivity based on adsorption for various materials,[7−12] including porous carbon materials,[4,13] zeolites,[14−16] and metal−organic frameworks (MOFs).[3,17−22] Various methods have also been proposed to simulate the gas transport and separation in nanopores,[6,23] including the external force (EF) method, the boundary driven (BD) method, and the dual control volume−grand canonical molecular dynamics (DCV-GCMD) method.[24] The EF method performs an external force field on each atom in the simulation box with periodic boundary conditions to achieve an equivalent pressure gradient in an infinite pore.[25,26] Ho and Striolo[27] have studied the transport of a mixture of methane and water through slit muscovite nanopores. The pressure gradient in the BD method is generated by means of the specific actions on the boundary, such as the moving "piston",[28] the external force within a specific region,[29] and the virtual semimembrane.[26,30] The DCV-GCMD method is a hybrid technique of grand canonical Monte Carlo (GCMC) and molecular dynamics (MD) simulations.[31−33] It contains two control volumes (CVs) at the upstream side (feed side) and the downstream side (permeate side) of the slit pore, with different pressures or chemical potentials. The simulation is carried out with an alternation of the Monte Carlo (MC) steps and the MD steps based on the MC/MD ratio. Due to the stability of simulation and the similarity to physical processes, the DCV-GCMD is widely used in gas transport simulation.

Various studies of single-component flow with the DCV-GCMD method have been carried out.[29,33−36] The flow rates in 2 nm slit pores have been measured to be 1 to 2 orders of magnitude higher than the predictions by the Knudsen diffusion. Jin and Firoozabadi[34] performed the flow of single-component species in the slit nanopore to investigate the large disparity between measurements and the prediction from the Knudsen diffusion. They found that the flow of the high density adsorbed layer contributes to flow enhancement. For the multicomponent gas transport, much effort has been devoted to developing effective algorithms and investigating the separation factor of advanced materials. Xu et al.[37]

Received: May 24, 2018
Revised: August 9, 2018
Published: August 14, 2018

DOI: 10.1021/acs.jpcc.8b04976
J. Phys. Chem. C 2018, 122, 20727−20735

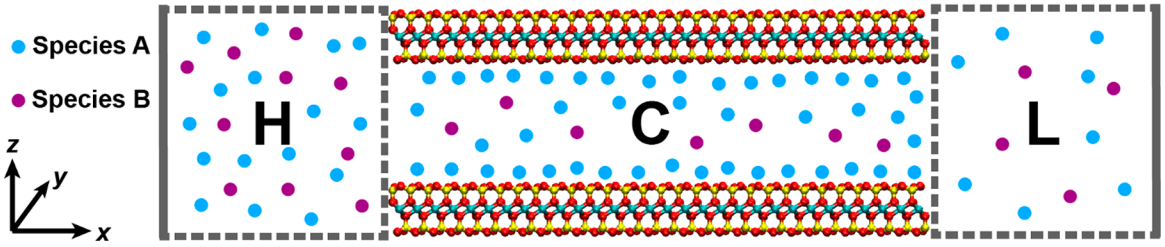

Figure 1. Sketch of the model configuration used in gas mixture transport in slit nanopores with the dual control volume.

performed the binary gas mixture transport through a structureless carbon slit pore by the DCV-GCMD simulations. To improve the efficiency for the simulation of alkanes, the configurational-bias MC was also proposed.[38−40] These methods have been widely utilized to simulate the gas mixture transport through various materials, such as graphitic slit pores,[1,2,23,41−46] carbon nanotubes,[47] nanoporous carbons with complex pore networks,[38,48−50] zeolites,[51] and silicon−carbide membranes.[52,53] In the conventional method, the chemical potential or partial pressure of each component is maintained by the GCMC method. The value of target chemical potential is obtained using equation of state (EOS) based on pressure, gas species, and compositions. One has to assign the compositions of gas mixture in the system before launching the simulation. The compositions are often set the same at both the feed side and the permeate side, which is kept constant in each control volume despite the fact that selectivity of the substrate may lead to different compositions. This assumption will lead to the inconsistency of the flux ratio between the two components in the pore and produced composition ratio in the permeate side.

Generally, the pressure at the permeate side should be set, but the composition is unknown. In GCMC simulations, the composition in each control volume should be known before launching the simulation to calculate the chemical potentials. The conventional method, namely, DCV-GCMD, cannot be used to simulate the condition of constant pressure with unknown composition in the permeate side for gas mixtures transport. Wang et al.[6] have proposed an iteration workflow based on the conventional method. The computational cost of each loop from the iteration method is similar to one complete run of the conventional DCV-GCMD simulation. The computations are time-consuming, and the stability of computations should be managed carefully.[6] Phan et al.[54] have simulated the H_2S/CH_4 mixture transport through a membrane containing water. The molecules in the permeate side are removed in different time intervals, which can model the condition close to vacuum. Cabrales-Navarro et al.[55] applied a similar method for vacuum conditions as well as a dynamic process of gas mixture transport with canonical ensemble. Because the parameters in the two control volumes are changing with time, one cannot determine the boundary conditions for macroscopic analysis. An accurate and efficient method will facilitate the molecular simulation of gas mixture transport and separation in nanopores.

In this work, we introduce a method to simulate gas mixture transport and separation in slit nanopores. In the Methodology Section, the molecular model and the methods of gas mixture transport are introduced, including conventional method, iterative method, and our proposed approach. In the Method Validation Section, our approach is validated by methane transport with marked components. The results from the conventional method, the iterative method, and the proposed method are compared. In the Application and Discussion Section, we use our proposed method to perform the simulations of CH_4/He and CO_2/CH_4 mixture transport through slit pores made of graphite, graphene, and tetrahedral−octahedral−tetrahedral (TOT) structures. The effects of various parameters on separation are discussed. The conclusions are drawn in the Conclusions Section.

METHODOLOGY

Model Description. A schematic representation of the system of this study is shown in Figure 1. The simulation box consists of three regions. The H-CV, L-CV, and C-regions correspond to the high-pressure CV at the upstream side (feed side), the low-pressure CV at the downstream side (permeate side), and the slit nanopore in the middle, respectively. The periodic boundary condition is applied in the *y*- and *z*-directions, while the fixed boundary condition is applied in the *x*-direction by means of a virtual reflective wall. Flow is along the *x*-direction. We performed simulations with three different solid structures including graphene, graphite (three sheets), and tetrahedral−octahedral−tetrahedral (TOT) structure from pyrophyllite (see Figure 2). The tetrahedral−octahedral−

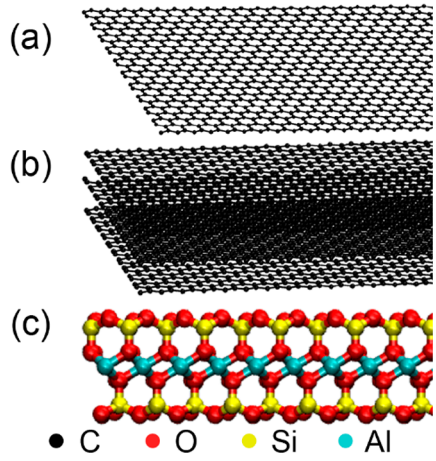

Figure 2. Molecular structure of the solid substrates of the slit pores. (a) Graphene, (b) graphite, and (c) tetrahedral−octahedral−tetrahedral (TOT) structure of clay mineral.

tetrahedral (TOT) structure exists in many clay minerals, which can represent the main properties of ideal Si−O surface in clays and construct the symmetric slit pore.

The solid substrates are fixed in the C-region which are parallel to the *xy*-plane. The pore lengths are 10.00, 30.12, and 90.36 nm in different settings. The pore width ranges from 0.80 to 10.00 nm. The widths in the *y*-direction are 4.47, 4.47, and 5.44 nm for graphene, graphite, and TOT, respectively.

DOI: 10.1021/acs.jpcc.8b04976
J. Phys. Chem. C 2018, 122, 20727−20735

For H- and the L-CVs, the domain size in the x- and y-directions is 30.00 nm × 4.47 nm, while the domain size in the z-direction will change with the settings for different pore widths. The gas molecules are modeled as the Lennard–Jones (LJ) fluid. The interactions between the gas–gas and the gas–solid particles i and j are modeled with the cut and shifted (CS) LJ 12-6 potential

$$\phi_{ij}^{CS} = \begin{cases} \phi_{ij}(r_{ij}) - \phi_{ij}(r_{cut}) & r_{ij} \le r_{cut} \\ 0 & r_{ij} > r_{cut} \end{cases} \quad (1)$$

where

$$\phi_{ij}(r_{ij}) = 4\varepsilon_{ij}\left[\left(\frac{\sigma_{ij}}{r_{ij}}\right)^{12} - \left(\frac{\sigma_{ij}}{r_{ij}}\right)^{6}\right] \quad (2)$$

The cutoff distance r_{cut} is set as 1 nm in this study. The effective LJ size and the energy parameters, σ and ε, are listed in Table 1.[44,56] For all the cross-term LJ parameters, the Lorentz–Berthelot mixing rules are employed.

Table 1. Parameters for LJ (12-6) potential[44,56]

	σ (nm)	ε/k_B (K)
CH_4	0.381	148.1
He	0.255	10.2
CO_2	0.379	225.3
C (graphene/graphite)	0.340	28.0
O (TOT)	0.317	78.2
Si (TOT)	0.395	47.8
Al (TOT)	0.411	32.7

The simulations are performed based on the open-source package LAMMPS,[57] with the additional function of the proposed method developed by the authors. The time step for MD simulation ranges from 1 to 5 fs depending on the case. We use 25 ns simulation time for the system to reach steady state and another 25 ns simulation time to calculate the density and pressure. The simulation time is extended to 50 ns for each process in the slit pore less than 1.00 nm width. The snapshots are taken every 0.5 ps for density and velocity calculation. At every 0.5 ns, the average properties are recorded for the calculation of mean value and standard deviation. The Nose–Hoover thermostat is performed for the entire domain at 298 K except the simulations for examining the effect of temperature.

Conventional and Iterative Methods. In the conventional DCV-GCMD, the pressure is maintained by performing a sufficient number of MC attempts, including insertions and deletions of molecules. For component i, the probability of acceptance for insertion is given by

$$p_i^+ = \min\left\{\frac{Z_i V}{N_i + 1}\exp\left(-\frac{\Delta U}{k_B T}\right), 1\right\} \quad (3)$$

where $Z_i = \exp(\mu_i/k_B T)/\Lambda_i^3$ is the absolute activity at temperature T; Λ_i is the de Broglie wavelength; k_B is the Boltzmann's constant; μ_i is the chemical potential; V is the volume of the CV; N_i is the number of molecules; and ΔU is the potential energy change resulting from inserting or deleting the molecule. When the insertion is accepted, the velocity of the molecule is assigned based on the Maxwell–Boltzmann distribution. The probability of acceptance for deletion is given by

$$p_i^- = \min\left\{\frac{N_i}{Z_i V}\exp\left(-\frac{\Delta U}{k_B T}\right), 1\right\} \quad (4)$$

The MC moves in each CV are followed by one MD step. The MC/MD ratio is set to 10 in this study.

The iterative method is a modified approach based on the conventional DCV-GCMD.[6] It resets the chemical potential in the L-CV based on the flux ratio of the two species in each loop. The iteration process will continue until the flux ratio in the nanopore and the mole ratio in the L-CV converge to the same value.

Proposed Method. At many experimental conditions and in many industrial processes, the pressure at the permeate side is not zero. The target chemical potentials in the H-CV can be obtained based on the feed composition and pressure. Then, the chemical potentials in the H-CV can be maintained by the conventional GCMC method. In the H-CV, the molecule exchanges come from the insertion and deletion by MC steps and the net flux between the H-CV and C-region. However, in the L-CV, because the composition is unknown, the chemical potential cannot be determined before launching the simulation. As a result, the insertion attempt cannot be performed in the conventional GCMC simulation. The molecule exchanges are from the molecule deletion in MC steps and the net flux between the L-CV and C-region. The removal of the molecules in the MC step is the key step in our proposed method.

The workflow is shown in Figure 3. We check for pressure in the L-CV during a given time interval. When the current

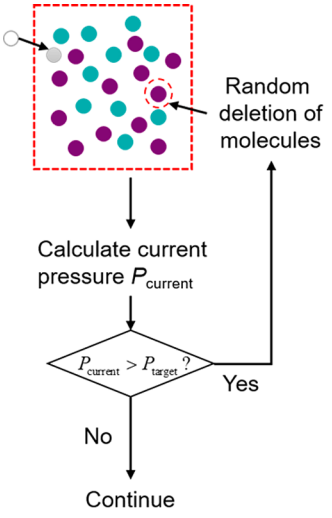

Figure 3. Pressure control in the permeate side.

pressure $P_{current}$ is higher than the target pressure P_{target}, we remove one molecule randomly at a time to reach the target pressure. In each step the random removal is independent of the previous steps. The target pressure is treated as a threshold value. Every molecule in the L-CV has the same probability to be picked up. However, because a reliable current pressure should be calculated with the information from many time steps, a time window should be assigned for pressure calculation. For the initial period, the time window is set the same as the current simulation time, which is shorter than the

DOI: 10.1021/acs.jpcc.8b04976
J. Phys. Chem. C 2018, 122, 20727–20735

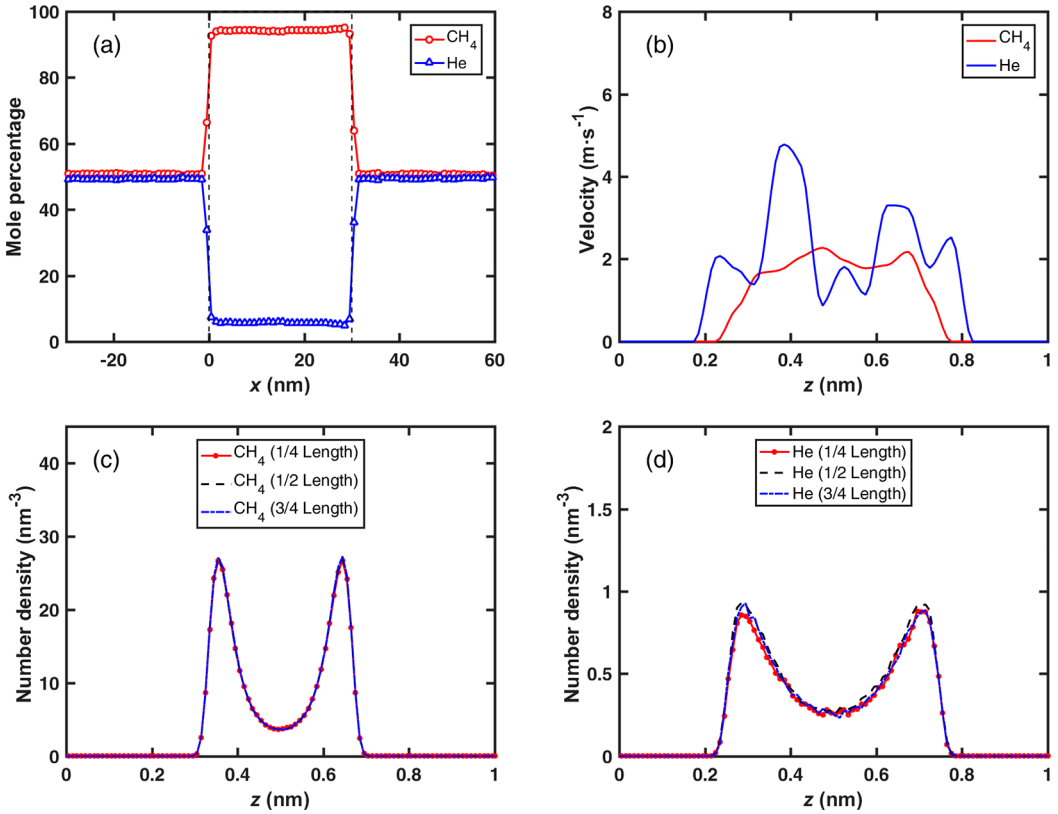

Figure 4. Simulation of the CH_4/He gas mixture transport by the conventional method: graphite slit pores; pore width = 1.00 nm; pore length = 30.12 nm; pressure gradient = 0.33 bar/nm; pressure = 60 bar in the H-CV; pressure = 50 bar in the L-CV; temperature = 298 K. (a) Composition along the *x*-direction. (b) Velocity in the *x*-direction at the middle of the slit pore. Molecular number density of CH_4 (c) and He (d) along the *z*-direction at three locations in the pore.

assigned value of the time window (see Figure S1). $P_{current}$ is usually zero in the early period because the initial condition is vacuum. In our approach, we define the separation factor as

$$S_{AB} = \frac{c_{L,A}/c_{L,B}}{c_{H,A}/c_{H,B}} \quad (5)$$

where c is the molar concentration; the subscripts H and L denote the H- and the L-CVs, respectively; and A and B denote Species A and Species B, respectively. Note that in our method in each step the random removal is independent of the previous steps.

METHOD VALIDATION

Simulation with Marked Component. To validate the proposed method, we performed the simulation without pressure difference between the H-CV and the L-CV first. The simulation was carried out in the graphene slit pore with the length of 30.12 nm and the pore width of 2.00 nm. The flow of single component gas was investigated, while the gas molecules were marked as two different species with the property of methane, namely, Species A and Species B. The pressures in the H-CV and the L-CV were set as 40 bar. The feed composition in the H-CV was maintained by the GCMC method with 70% Species A and 30% Species B in mole percentage. If the method is valid, the composition in each region should be uniform, and the number density in the H-CV and the L-CV should be the same. The result in Figure S2(a) is the average composition in each region. The number density in Figure S2(b) and the mole percentage in Figure S2(c) are the average values in each cross-section, including the adsorbed layer. The time window for pressure monitoring was set as 5 ps, which should be compatible with the MC/MD ratio. Otherwise, it may lead to a delay response of current pressure or have significant fluctuations.

A simulation with pressure difference was also performed in the same configuration as above; the pressure in the L-CV is 30 bar instead of 40 bar. The velocity in the *y*- and *z*-directions was taken into account for temperature calculation. The composition in each region should be uniform as well. The results are as expected (see Figure S3).

Comparison of Results from the Conventional Method and Proposed Method. The transport of the CH_4/He mixture was investigated in the graphite slit pore with the length of 30.12 nm and the pore width of 1.00 nm. The pressure is set as 60 and 50 bar in the H-CV and the L-CV, respectively. The feed composition of each component was 0.5 in mole fraction for the two methods in the H-CV. In the L-CV, the composition of each component was set as 0.5 in mole fraction in the conventional method as well, while in our method the composition was determined from the simulation.

The results are presented in Figures 4 and 5. In the conventional method, the composition is kept constant in both the H-CV and the L-CV. In our method, the composition in the L-CV shows significant difference from the feed composition due to the separation in the slit nanopore. The solid substrate selectively adsorbs CH_4, which has a higher number density and a higher mole percentage than He. In the conventional method, the mole percentage is uniform in each region. In our method, the mole percentage of CH_4 in the pore

DOI: 10.1021/acs.jpcc.8b04976
J. Phys. Chem. C 2018, 122, 20727−20735

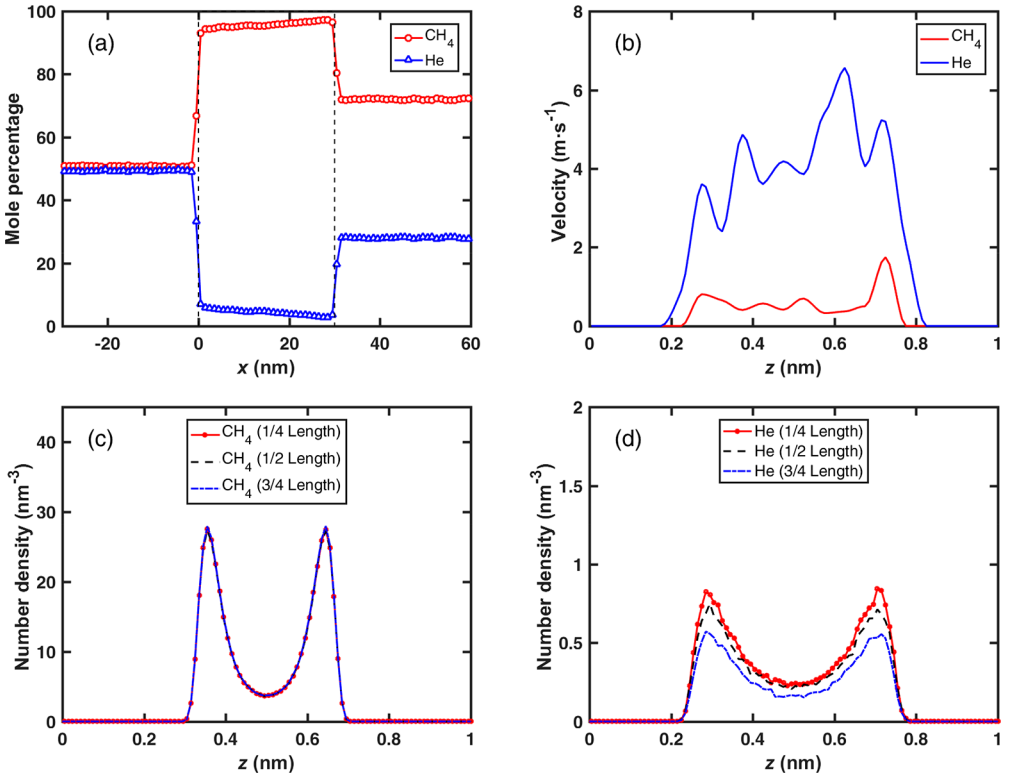

Figure 5. Simulation of the CH_4/He gas mixture transport by the proposed method: graphite slit pores; pore width = 1.00 nm; pore length = 30.12 nm; pressure gradient = 0.33 bar/nm; pressure = 60 bar in the H-CV; pressure = 50 bar in the L-CV; temperature = 298 K. (a) Composition along the *x*-direction. (b) Velocity in the *x*-direction at the middle of the slit pore. Molecular number density of CH_4 (c) and He (d) along the *z*-direction at three locations in the pore.

exhibits slight increasing trend along the flow direction. Helium has the opposite trend. The molecule number density profiles at the locations of 1/4, 1/2, and 3/4 of the pore length have minor differences as well. The velocity profiles reveal a pronounced difference between the two methods. The velocity profiles of CH_4 and He are very close to each other in the conventional method, whereas the velocity of He is much higher than CH_4 in our method. The concentration difference of He between the feed side and permeate side is underestimated in the conventional method because the mole percentage of He is much lower in the permeate side due to the selectivity of the pore. Therefore, He should have larger driving force for the gas transport, just like in the proposed method (see Figure 5(b)), which will lead to higher He velocity than CH_4. Graphite has an extremely smooth surface, and then each component has pronounced slip velocity which will lead to substantial mobility near the solid surface. As a result, the adsorption has a significant contribution to the total flux. The separation factor is related to the coupled effect between the two factors: one is the enhanced flux for the preferred component due to adsorption, and the other is the higher concentration difference for the less adsorbed component. We also performed the comparative simulations for the two methods in nanopores with the widths of 2.00 and 10.00 nm. The results reveal much lower selectivity of the 2.00 nm pore and almost no selectivity of the 10.00 nm pore (Figures S4–S7).

Comparison of the Iterative Method and Proposed Method. We have compared the performance of the iterative method and our proposed method using the data for example in Figure 5. The parameters in the iterative method were set the same as the conventional method except for the chemical potentials in the L-CV. In the iterative method, the composition in the permeate side is set the same as in the feed side in the first iteration. Based on the flux, in the subsequent iterations, the composition in the permeate side is updated, and the flux ratio is then computed for the next iteration. The process of the iterative method is presented in Figure 6. The mole ratio in the L-CV (same as the separation factor S_{AB}) from the proposed method is presented using the

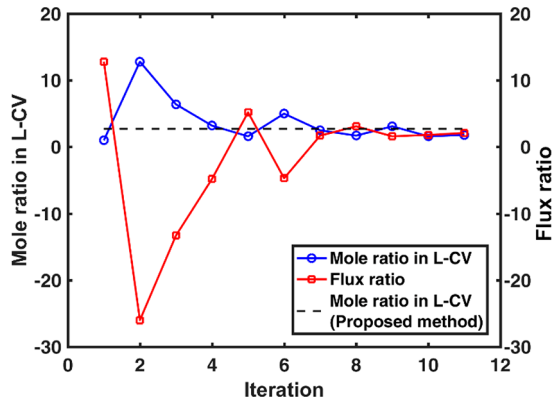

Figure 6. Mole ratio of CH_4/He in the L-CV and flux ratio in the slit nanopore from the iterative method. The mole ratio in the L-CV (separation factor S_{AB}) from the proposed method is presented using a dashed line as a reference. Graphite slit pores; pore width = 1.00 nm; pore length = 30.12 nm; pressure gradient = 0.33 bar/nm; pressure = 60 bar in the H-CV; pressure = 50 bar in the L-CV; temperature = 298 K.

DOI: 10.1021/acs.jpcc.8b04976
J. Phys. Chem. C 2018, 122, 20727−20735

dashed line as a reference. The flux ratio and mole ratio converge to the same value after 11 iterations. The results from the iterative method agree with the results from our proposed method. We noticed convergence issues in the iterative method. In some iterations, there were negative flux ratios. We cut back the mole ratio in the L-CV for the next iteration to reduce the convergence issue (see the second to fourth iterations in Figure 6). The convergence problems in the iterative method have been discussed by Wang et al.[6]

We used the workstation with two Intel Xeon 2690 v4 CPUs and two Nvidia P100 GPUs to compare the computational efficiency. It took 71 h 44 min 28 s for the entire simulation of the proposed method. One iteration of the iterative method took 78 h 15 min 27 s. The number of iterations may vary in different systems. For this particular example, there were 11 iterations to achieve the convergence, and then our approach is about 12 times faster than the iterative method.

APPLICATION AND DISCUSSION

Three solid structures, including graphene, graphite, and TOT, were selected for investigation of transport and separation. Graphene and graphite have the same surface structure but different strengths for adsorption. The three layers of graphitic sheets can provide stronger interaction with the gas molecules than in graphene. The TOT surface has a different molecular structure and pairwise interaction which has a rougher surface than graphene and graphite.

First, we performed the simulations for the CH_4/He mixture in the slit pores with different widths ranging from 0.80 to 10.00 nm. The pore length is 30.12 nm. The pressure was set as 60 and 50 bar in the H-CV and the L-CV, respectively. The rest of the model configurations were the same as in the Method Validation Section. The separation factor was calculated from eq 5. The results are presented in Figure 7.

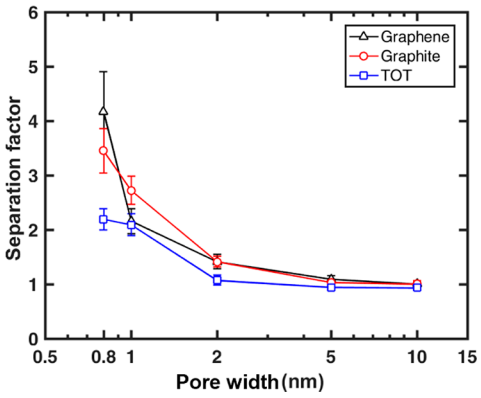

Figure 7. Separation factor of the CH_4/He mixture vs pore width in three slit pores: pore length = 30.12 nm; pressure gradient = 0.33 bar/nm; pressure = 60 bar in the H-CV; pressure = 50 bar in the L-CV; temperature = 298 K. Simulations based on the proposed method.

The separation factor increases significantly with the decrease of pore width, especially below 1.00 nm. When the pore width is larger than 2.00 nm, the material can hardly provide selectivity. The trend of separation factor is mainly due to the coupled effect between the enhanced flux of CH_4 due to adsorption and the higher concentration difference of He due to selectivity. The flux from the adsorbed layer has much larger contribution to the total flux in the smaller pores than in the larger pores. The effect of higher concentration difference of He is relatively weak when the pore width is very small. The separation factors for the three substrates are close to one in pore widths greater than 5.00 nm, while it is enhanced in pore widths less than 1.00 nm. TOT shows less selectivity than the other two materials. These phenomena are mainly controlled by the effect of substrate surface roughness.

The simulations were performed in the slit pores with a width of 1.00 and 2.00 nm at different average pressures at the same pressure gradient of 0.33 bar/nm. The results show that the separation factor decreases with the average pressure increase in 1.00 nm pore width (see Figure 8(a)), due to less contribution at high pressure for flux from the adsorbed layer than at low pressure. However, there is almost no change with average pressure in the 2.00 nm pore (see Figure 8(b)). Extensive simulations for 10.00 nm pore width in graphite are also made (see Figure S8). There is no clear relationship between the separation factor and average pressure in the 10.00 nm pore width. There is almost no separation for the gas mixture. In the pore widths larger than 2.00 nm, the mobility of the adsorbed layer cannot provide pronounced contribution to the total flux, so that the separation factors as well as their changes are negligible. The results indicate that the average pressure may have a pronounced effect when the pore width is less than 1.00 nm. Graphene and graphite have different macroscopic interaction strengths with gas molecules, but the separation factors are very close. The separation factor of TOT is lower than the other two substrates. The surface roughness has a more pronounced effect than the interaction strength.

We also carried out the simulations for transport of the CO_2/CH_4 mixture in the three materials. The pressure gradient was 0.33 bar/nm. For the effect of pore width, the pressures were set as 40 and 30 bar in the H-CV and the L-CV, respectively. For the effect of average pressure, the pressures in the H-CV and the L-CV were adjusted to maintain the pressure gradient. The rest of the model configurations were the same as the CH_4/He gas mixture simulations. Due to the preferred adsorption of CO_2 instead of CH_4, the slit pores show selectivity for CO_2. The separation factors with respect to CO_2 in the mixture are presented in Figures 9 and 10. The results of 1.00 and 2.00 nm pore widths on composition, velocity profile, and number density are shown in Figures S9 and S10. Similar to the CH_4/He mixture, the separation factor shows a clear trend of the effect of pore width. The reason is related to the coupled effect of the enhanced flux of CO_2 due to selective adsorption and the higher concentration difference of CH_4 between the two sides due to the selectivity, which is similar to the CH_4/He mixture. When the pore width is larger than 5.00 nm, the material cannot provide pronounced selectivity, especially in TOT. The separation factors for graphite and graphene are still very close in pore widths larger than 2.00 nm, whereas they show differences in pore widths less than 1.00 nm. In the 1.00 nm pore width, the separation factor presents a minor downward trend as average pressure increases. The effect of average pressure is negligible in the 2.00 nm pore width. TOT has weaker selectivity than the other two materials in the whole range.

The effects of pore length, temperature, pressure gradient, and feed composition are also investigated. The details and results are provided in the Supporting Information (see Figures S11 and S12).

DOI: 10.1021/acs.jpcc.8b04976
J. Phys. Chem. C 2018, 122, 20727−20735

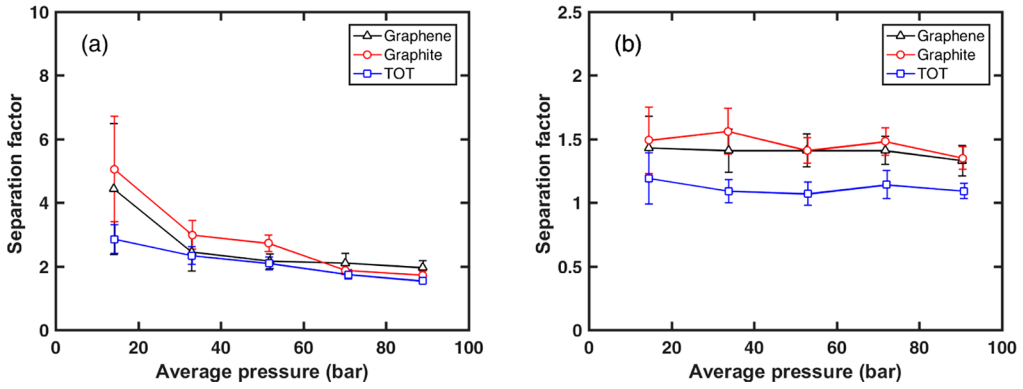

Figure 8. Separation factor of the CH_4/He mixture vs average pressure in three slit pores. (a) Pore width = 1.00 nm; (b) pore width = 2.00 nm; pore length = 30.12 nm; pressure gradient = 0.33 bar/nm; and temperature = 298 K. The pressures in the H-CV and the L-CV are assigned based on the average pressure, pressure gradient, and pore length. Simulations based on the proposed method.

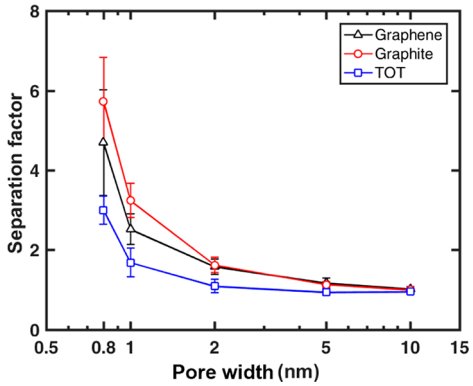

Figure 9. Separation factor of the CO_2/CH_4 mixture vs pore width in three slit pores: pore length = 30.12 nm; pressure gradient = 0.33 bar/nm; pressure = 40 bar in the H-CV; pressure = 30 bar in the L-CV; temperature = 298 K. Simulations based on the proposed method.

CONCLUSIONS

In this work, we have simulated separation of binary gas mixtures in slit nanopores. We introduce a new method based on the dual control volume−grand canonical molecular dynamics (DCV-GCMD) simulations. In our approach we directly compute the gas composition at the permeate side. Our method is based on random removal of molecules from the permeate side to keep the pressure constant. The inconsistency of the species flux ratio in the pore and the mole ratio of the produced fluid in the permeate side is eliminated. We improve the computational efficiency significantly compared to the iterative method. We used the proposed method to investigate flow and separation of binary mixtures of CH_4/He and CO_2/CH_4 in nanopores of various widths and length and three different slit pores. We compared the results from our method and the conventional method and the iterative method. The results from the iterative methods are the same as our proposed method. Our method is 1 order of magnitude faster. The main conclusions drawn from this work are:

(1) The composition in the permeate side is significantly different from the feed composition when the pore widths are less than 2.00 nm.

(2) There is a significant difference between the computed velocity of species in the nanopores from the conventional DCV-GCMD simulation and our method.

(3) The separation in molecularly nonsmooth nanopores is less than molecularly smooth nanopores.

ASSOCIATED CONTENT

Supporting Information

The Supporting Information is available free of charge on the ACS Publications website at DOI: 10.1021/acs.jpcc.8b04976.

Sensitivity analysis of various parameters and Figures S1−S12 (PDF)

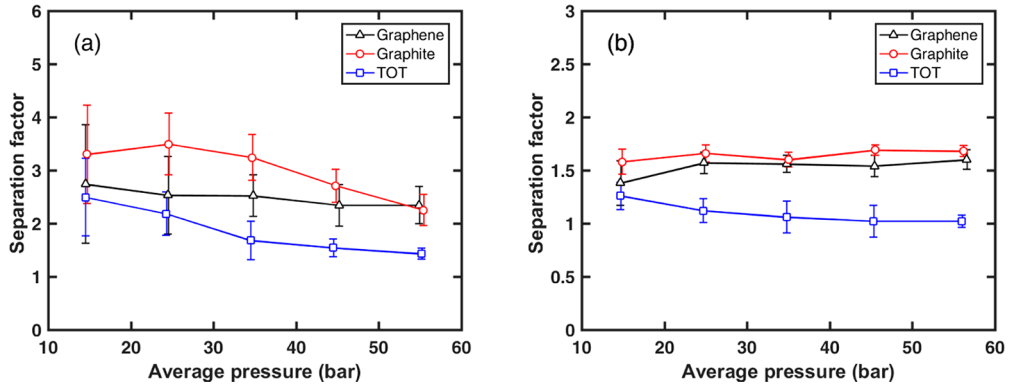

Figure 10. Separation factor of the CO_2/CH_4 mixture vs average pressure in three slit pores. (a) Pore width = 1.00 nm; (b) pore width = 2.00 nm; pore length = 30.12 nm; pressure gradient = 0.33 bar/nm; temperature = 298 K. The pressures in the H-CV and the L-CV are assigned based on the average pressure, pressure gradient, and pore length. Simulations based on the proposed method.

DOI: 10.1021/acs.jpcc.8b04976
J. Phys. Chem. C 2018, 122, 20727−20735

AUTHOR INFORMATION

Corresponding Author

*Tel.: 650-326-9172. Fax: 650-472-9285. E-mail: af@rerinst.org.

ORCID

Abbas Firoozabadi: 0000-0001-6102-9534

Notes

The authors declare no competing financial interest.

ACKNOWLEDGMENTS

This work was supported by the member companies of the Reservoir Engineering Research Institute (RERI). Their support is appreciated.

REFERENCES

(1) Xu, L.; Tsotsis, T. T.; Sahimi, M. Nonequilibrium Molecular Dynamics Simulation of Transport and Separation of Gases in Carbon Nanopores. I. Basic Results. *J. Chem. Phys.* **1999**, *111*, 3252−3264.

(2) Xu, L.; Sedigh, M. G.; Tsotsis, T. T.; Sahimi, M. Nonequilibrium Molecular Dynamics Simulation of Transport and Separation of Gases in Carbon Nanopores. II. Binary and Ternary Mixtures and Comparison with the Experimental Data. *J. Chem. Phys.* **2000**, *112*, 910−922.

(3) Yazaydın, A. O.; Benin, A. I.; Faheem, S. A.; Jakubczak, P.; Low, J. J.; Willis, R. R.; Snurr, R. Q. Enhanced CO2 Adsorption in Metal-Organic Frameworks Via Occupation of Open-Metal Sites by Coordinated Water Molecules. *Chem. Mater.* **2009**, *21*, 1425−1430.

(4) Liu, Y.; Wilcox, J. Molecular Simulation Studies of CO2 Adsorption by Carbon Model Compounds for Carbon Capture and Sequestration Applications. *Environ. Sci. Technol.* **2013**, *47*, 95−101.

(5) Venna, S. R.; Carreon, M. A. Highly Permeable Zeolite Imidazolate Framework-8 Membranes for CO2/CH4 Separation. *J. Am. Chem. Soc.* **2009**, *132*, 76−78.

(6) Wang, S.-M.; Yu, Y.-X.; Gao, G.-H. Grand Canonical Monte Carlo and Non-Equilibrium Molecular Dynamics Simulation Study on the Selective Adsorption and Fluxes of Oxygen/Nitrogen Gas Mixtures through Carbon Membranes. *J. Membr. Sci.* **2006**, *271*, 140−150.

(7) Thornton, A. W.; Dubbeldam, D.; Liu, M. S.; Ladewig, B. P.; Hill, A. J.; Hill, M. R. Feasibility of Zeolitic Imidazolate Framework Membranes for Clean Energy Applications. *Energy Environ. Sci.* **2012**, *5*, 7637−7646.

(8) Keskin, S.; Sholl, D. S. Selecting Metal Organic Frameworks as Enabling Materials in Mixed Matrix Membranes for High Efficiency Natural Gas Purification. *Energy Environ. Sci.* **2010**, *3*, 343−351.

(9) Watanabe, T.; Keskin, S.; Nair, S.; Sholl, D. S. Computational Identification of a Metal Organic Framework for High Selectivity Membrane-Based CO2/CH4 Separations: Cu (Hfipbb)(H2Hfipbb) 0.5. *Phys. Chem. Chem. Phys.* **2009**, *11*, 11389−11394.

(10) Kim, N.; Harale, A.; Tsotsis, T. T.; Sahimi, M. Atomistic Simulation of Nanoporous Layered Double Hydroxide Materials and Their Properties. II. Adsorption and Diffusion. *J. Chem. Phys.* **2007**, *127*, 224701.

(11) Lim, S. Y.; Tsotsis, T. T.; Sahimi, M. Molecular Simulation of Diffusion and Sorption of Gases in an Amorphous Polymer. *J. Chem. Phys.* **2003**, *119*, 496−504.

(12) Le, T.; Striolo, A.; Cole, D. R. CO2−C4H10 Mixtures Simulated in Silica Slit Pores: Relation between Structure and Dynamics. *J. Phys. Chem. C* **2015**, *119*, 15274−15284.

(13) Cao, D.; Wu, J. Modeling the Selectivity of Activated Carbons for Efficient Separation of Hydrogen and Carbon Dioxide. *Carbon* **2005**, *43*, 1364−1370.

(14) Liu, B.; Smit, B. Comparative Molecular Simulation Study of CO2/N2 and CH4/N2 Separation in Zeolites and Metal− Organic Frameworks. *Langmuir* **2009**, *25*, 5918−5926.

(15) Krishna, R.; Van Baten, J. Using Molecular Simulations for Screening of Zeolites for Separation of CO_2/CH_4 Mixtures. *Chem. Eng. J.* **2007**, *133*, 121−131.

(16) Dehghani, M.; Asghari, M.; Mohammadi, A. H.; Mokhtari, M. Molecular Simulation and Monte Carlo Study of Structural-Transport-Properties of Peba-Mfi Zeolite Mixed Matrix Membranes for CO2, CH4 and N2 Separation. *Comput. Chem. Eng.* **2017**, *103*, 12−22.

(17) Yang, Q.; Zhong, C. Molecular Simulation of Carbon Dioxide/Methane/Hydrogen Mixture Adsorption in Metal− Organic Frameworks. *J. Phys. Chem. B* **2006**, *110*, 17776−17783.

(18) Yang, Q.; Xue, C.; Zhong, C.; Chen, J. F. Molecular Simulation of Separation of CO2 from Flue Gases in Cu-Btc Metal-Organic Framework. *AIChE J.* **2007**, *53*, 2832−2840.

(19) Liu, B.; Smit, B. Molecular Simulation Studies of Separation of CO2/N2, CO2/CH4, and CH4/N2 by Zifs. *J. Phys. Chem. C* **2010**, *114*, 8515−8522.

(20) Bae, Y.-S.; Mulfort, K. L.; Frost, H.; Ryan, P.; Punnathanam, S.; Broadbelt, L. J.; Hupp, J. T.; Snurr, R. Q. Separation of CO2 from CH4 Using Mixed-Ligand Metal− Organic Frameworks. *Langmuir* **2008**, *24*, 8592−8598.

(21) Babarao, R.; Hu, Z.; Jiang, J.; Chempath, S.; Sandler, S. I. Storage and Separation of CO2 and CH4 in Silicalite, C168 Schwarzite, and Irmof-1: A Comparative Study from Monte Carlo Simulation. *Langmuir* **2007**, *23*, 659−666.

(22) Babarao, R.; Jiang, J. Unprecedentedly High Selective Adsorption of Gas Mixtures in Rho Zeolite-Like Metal− Organic Framework: A Molecular Simulation Study. *J. Am. Chem. Soc.* **2009**, *131*, 11417−11425.

(23) Firouzi, M.; Tsotsis, T. T.; Sahimi, M. Nonequilibrium Molecular Dynamics Simulations of Transport and Separation of Supercritical Fluid Mixtures in Nanoporous Membranes. I. Results for a Single Carbon Nanopore. *J. Chem. Phys.* **2003**, *119*, 6810−6822.

(24) Arya, G.; Chang, H.-C.; Maginn, E. J. A Critical Comparison of Equilibrium, Non-Equilibrium and Boundary-Driven Molecular Dynamics Techniques for Studying Transport in Microporous Materials. *J. Chem. Phys.* **2001**, *115*, 8112−8124.

(25) Falk, K.; Coasne, B.; Pellenq, R.; Ulm, F.-J.; Bocquet, L. Subcontinuum Mass Transport of Condensed Hydrocarbons in Nanoporous Media. *Nat. Commun.* **2015**, *6*, 6949.

(26) Wu, T.; Zhang, D. Impact of Adsorption on Gas Transport in Nanopores. *Sci. Rep.* **2016**, *6*, 23629.

(27) Ho, T. A.; Striolo, A. Water and Methane in Shale Rocks: Flow Pattern Effects on Fluid Transport and Pore Structure. *AIChE J.* **2015**, *61*, 2993−2999.

(28) Riewchotisakul, S.; Akkutlu, I. Y. Adsorption-Enhanced Transport of Hydrocarbons in Organic Nanopores. *SPE J.* **2016**, *21*, 1960−1969.

(29) Collell, J.; Galliero, G.; Vermorel, R.; Ungerer, P.; Yiannourakou, M.; Montel, F.; Pujol, M. Transport of Multicomponent Hydrocarbon Mixtures in Shale Organic Matter by Molecular Simulations. *J. Phys. Chem. C* **2015**, *119*, 22587−22595.

(30) Li, J.; Liao, D.; Yip, S. Coupling Continuum to Molecular-Dynamics Simulation: Reflecting Particle Method and the Field Estimator. *Phys. Rev. E: Stat. Phys., Plasmas, Fluids, Relat. Interdiscip. Top.* **1998**, *57*, 7259.

(31) Allen, M. P.; Tildesley, D. *J. Computer Simulation of Liquids*, 1st ed.; Oxford University Press: New York, 1989.

(32) Frenkel, D.; Smit, B. *Understanding Molecular Simulation: From Algorithms to Applications*; Academic Press, 2001; Vol. *1*.

(33) Cracknell, R. F.; Nicholson, D.; Quirke, N. Direct Molecular Dynamics Simulation of Flow Down a Chemical Potential Gradient in a Slit-Shaped Micropore. *Phys. Rev. Lett.* **1995**, *74*, 2463.

(34) Jin, Z.; Firoozabadi, A. Flow of Methane in Shale Nanopores at Low and High Pressure by Molecular Dynamics Simulations. *J. Chem. Phys.* **2015**, *143*, 104315.

(35) Jin, Z.; Firoozabadi, A. Phase Behavior and Flow in Shale Nanopores from Molecular Simulations. *Fluid Phase Equilib.* **2016**, *430*, 156−168.

DOI: 10.1021/acs.jpcc.8b04976
J. Phys. Chem. C 2018, 122, 20727−20735

(36) Pohl, P. I.; Heffelfinger, G. S. Massively Parallel Molecular Dynamics Simulation of Gas Permeation across Porous Silica Membranes. *J. Membr. Sci.* **1999**, *155*, 1−7.
(37) Xu, L.; Sedigh, M. G.; Sahimi, M.; Tsotsis, T. T. Non-equilibrium Molecular Dynamics Simulation of Transport of Gas Mixtures in Nanopores. *Phys. Rev. Lett.* **1998**, *80*, 3511−3514.
(38) Firouzi, M.; Sahimi, M. Molecular Dynamics Simulation of Transport and Separation of Carbon Dioxide−Alkane Mixtures in a Nanoporous Membrane under Sub-and Supercritical Conditions. *Transp. Porous Media* **2016**, *115*, 495−518.
(39) Firouzi, M.; Tsotsis, T. T.; Sahimi, M. Molecular Dynamics Simulations of Transport and Separation of Supercritical Carbon Dioxide-Alkane Mixtures in Supported Membranes. *Chem. Eng. Sci.* **2007**, *62*, 2777−2789.
(40) Firouzi, M.; Nezhad, K. M.; Tsotsis, T. T.; Sahimi, M. Molecular Dynamics Simulations of Transport and Separation of Carbon Dioxide−Alkane Mixtures in Carbon Nanopores. *J. Chem. Phys.* **2004**, *120*, 8172−8185.
(41) Sedigh, M. G.; Onstot, W. J.; Xu, L.; Peng, W. L.; Tsotsis, T. T.; Sahimi, M. Experiments and Simulation of Transport and Separation of Gas Mixtures in Carbon Molecular Sieve Membranes. *J. Phys. Chem. A* **1998**, *102*, 8580−8589.
(42) Seo, Y. G.; Kum, G. H.; Seaton, N. A. Monte Carlo Simulation of Transport Diffusion in Nanoporous Carbon Membranes. *J. Membr. Sci.* **2002**, *195*, 65−73.
(43) Wu, Z.; Liu, Z.; Wang, W.; Fan, Y.; Xu, N. Non-Equilibrium Molecular Dynamics Simulation on Permeation and Separation of H2/CO in Nanoporous Carbon Membranes. *Sep. Purif. Technol.* **2008**, *64*, 71−77.
(44) Firouzi, M.; Wilcox, J. Molecular Modeling of Carbon Dioxide Transport and Storage in Porous Carbon-Based Materials. *Microporous Mesoporous Mater.* **2012**, *158*, 195−203.
(45) Firouzi, M.; Wilcox, J. Slippage and Viscosity Predictions in Carbon Micropores and Their Influence on CO2 and CH4 Transport. *J. Chem. Phys.* **2013**, *138*, 064705.
(46) Travis, K. P.; Gubbins, K. E. Transport Diffusion of Oxygen−Nitrogen Mixtures in Graphite Pores: A Nonequilibrium Molecular Dynamics (NEMD) Study. *Langmuir* **1999**, *15*, 6050−6059.
(47) Düren, T.; Keil, F. J.; Seaton, N. A. Composition Dependent Transport Diffusion Coefficients of CH4/CF4Mixtures in Carbon Nanotubes by Non-Equilibrium Molecular Dynamics Simulations. *Chem. Eng. Sci.* **2002**, *57*, 1343−1354.
(48) Xu, L.; Sahimi, M.; Tsotsis, T. T. Nonequilibrium Molecular Dynamics Simulations of Transport and Separation of Gas Mixtures in Nanoporous Materials. *Phys. Rev. E: Stat. Phys., Plasmas, Fluids, Relat. Interdiscip. Top.* **2000**, *62*, 6942−6948.
(49) Düren, T.; Jakobtorweihen, S.; Keil, F. J.; Seaton, N. A. Grand Canonical Molecular Dynamics Simulations of Transport Diffusion in Geometrically Heterogeneous Pores. *Phys. Chem. Chem. Phys.* **2003**, *5*, 369−375.
(50) Kaganov, I.; Sheintuch, M. Nonequilibrium Molecular Dynamics Simulation of Gas-Mixtures Transport in Carbon-Nanopore Membranes. *Phys. Rev. E: Stat. Phys., Plasmas, Fluids, Relat. Interdiscip. Top.* **2003**, *68*, 046701.
(51) Newsome, D. A.; Sholl, D. S. Predictive Assessment of Surface Resistances in Zeolite Membranes Using Atomically Detailed Models. *J. Phys. Chem. B* **2005**, *109*, 7237−7244.
(52) Rajabbeigi, N.; Tsotsis, T. T.; Sahimi, M. Molecular Pore-Network Model for Nanoporous Materials. II: Application to Transport and Separation of Gaseous Mixtures in Silicon-Carbide Membranes. *J. Membr. Sci.* **2009**, *345*, 323−330.
(53) Naserifar, S.; Tsotsis, T. T.; Goddard, W. A., III; Sahimi, M. Toward a Process-Based Molecular Model of Sic Membranes: III. Prediction of Transport and Separation of Binary Gaseous Mixtures Based on the Atomistic Reactive Force Field. *J. Membr. Sci.* **2015**, *473*, 85−93.
(54) Phan, A.; Cole, D. R.; Weiß, R. G.; Dzubiella, J.; Striolo, A. Confined Water Determines Transport Properties of Guest Molecules in Narrow Pores. *ACS Nano* **2016**, *10*, 7646−7656.
(55) Cabrales-Navarro, F. A.; Gómez-Ballesteros, J. L.; Balbuena, P. B. Molecular Dynamics Simulations of Metal-Organic Frameworks as Membranes for Gas Mixtures Separation. *J. Membr. Sci.* **2013**, *428*, 241−250.
(56) Bhatia, S. K.; Bonilla, M. R.; Nicholson, D. Molecular Transport in Nanopores: A Theoretical Perspective. *Phys. Chem. Chem. Phys.* **2011**, *13*, 15350−15383.
(57) Plimpton, S. Fast Parallel Algorithms for Short-Range Molecular Dynamics. *J. Comput. Phys.* **1995**, *117*, 1−19.

DOI: 10.1021/acs.jpcc.8b04976
J. Phys. Chem. C 2018, 122, 20727−20735